Measurement of poloidal velocity on the National Spherical Torus Experiment (invited)[a)]

Ronald E. Bell[b)] and Russell Feder
Princeton Plasma Physics Laboratory, Princeton, New Jersey 08543, USA

(Presented 18 May 2010; received 17 May 2010; accepted 26 July 2010; published online 20 October 2010)

A diagnostic suite has been developed to measure the impurity poloidal flow using charge exchange recombination spectroscopy on the National Spherical Torus Experiment. Toroidal and poloidal viewing systems measure all the quantities required to determine the radial electric field. Two sets of up/down symmetric poloidal views are used to measure both the active emission in the plane of the neutral heating beams and the background emission in a radial plane away from the neutral beams. Differential velocity measurements isolate the line-integrated poloidal velocity from apparent flows due to the energy-dependent charge exchange cross section. Six $f/1.8$ spectrometers measure 276 spectra to obtain 75 active and 63 background channels every 10 ms. The local measurements from a similar midplane toroidal viewing system are mapped into two dimensions to allow the inversion of poloidal line-integrated measurements to obtain local poloidal velocity profiles. The radial resolution after inversion is 0.6–1.8 cm from the plasma edge to the center. [doi:10.1063/1.3485027]

I. INTRODUCTION

Poloidal velocity (v_θ) is arguably the most challenging of the quantities measured with charge exchange recombination spectroscopy in magnetically confined plasmas. The small magnitude of the poloidal velocity compared to the toroidal velocity is one reason. Another results from atomic physics effects, which are further complicated by the gyromotion of the ions. The geometry of the neutral heating beams can be another complication; if the beam height is large, a line-integrated instead of local measurement will result.

Typically, the poloidal velocity is much smaller than the toroidal velocity (v_ϕ) in a tokamak plasma, $v_\theta \ll v_\phi$, requiring more accuracy in the measurement of v_θ. On the National Spherical Torus Experiment (NSTX), for example, the toroidal velocity has been measured up to 350 km/s, while the poloidal velocity is a few km/s. The large ratio between the two requires that the viewing direction of a poloidal viewing sightline be known quite accurately to eliminate errors due to contributions from the toroidal velocity components in the poloidal viewing optics.

Measurements with charge exchange recombination spectroscopy are affected by the energy dependence of the cross section for charge exchange between the beam neutrals and the impurity ions of interest. For a Maxwellian velocity distribution of impurity ions and a monodirectional neutral beam, the collision energy will depend on whether the ion is moving toward or away from the beam. This will be exaggerated with toroidal flow. Consider a charge exchange cross section that increases with increasing collision energy. The impurity ions in the distribution moving toward the beam (with a velocity component antiparallel to the beam neutral trajectory) will more likely undergo charge exchange than those moving away from the beam (with a velocity component parallel to the beam neutral trajectory). This will result in a net flow toward the neutral beam for the product ions of the charge exchange interaction. Since it is the product ions that are measured, any view with a component in the direction of the neutral beam will observe an extra velocity not associated with the velocity of the original distribution. With hydrogenic neutral beams and positive neutral beam ion sources, there are full, half, and third energy components of the beam neutrals due to the molecular nature of the gas in the neutral beam source. Contributions for all of these components, each with differing charge exchange cross sections, will contribute to the apparent velocity measured. The net flow toward the beam will increase with increasing ion temperature. The population of product ions will also vary around the gyro orbit since the collision energy depends on the location of the impurity ion in its gyro orbit.[1] The direction of the net flow, originally directed at the neutral beam, will rotate with the gyromotion of the ions. For a finite lifetime of the excited state of the product ion, a vertical component of the net flow will result. This component of velocity will increase with ion temperature and magnetic field and can be large compared to the actual poloidal velocity of the original distribution. On the Tokamak Fusion Test Reactor (TFTR), this gyro orbit finite lifetime effect produced apparent vertical velocities not associated with poloidal velocity up to 40 km/s. NSTX has ion temperatures and magnetic fields that are each lower by more than an order of magni-

[a)] Invited paper, published as part of the Proceedings of the 18th Topical Conference on High-Temperature Plasma Diagnostics, Wildwood, New Jersey, May 2010.

[b)] Author to whom correspondence should be addressed. Electronic mail: rbell@pppl.gov.

tude from TFTR, so apparent velocities from this effect are less than 0.2 km/s and can be neglected here.

The strength of charge exchange recombination spectroscopy is the ability to provide local measurements of ion temperature, toroidal velocity, and impurity density profiles since charge exchange emission is located in the beam volume. The radial resolution for toroidal views can be optimized if the sightlines are tangent to the magnetic flux surfaces where they intersect the volume of the neutral beam. Typically, the beam width is small compared to the plasma major radius, so spatial resolution of the order of 1 cm or better can be readily achieved. For poloidal views, one must consider the height of the beam compared to the local minor radius when determining radial resolution. The neutral heating beams are often taller than wide. As vertical views approach the magnetic axis, the radial resolution deteriorates to the beam height divided by the local plasma elongation. The poloidal viewing measurements are more likely to be line-integrated than local.

There are three main elements to the design strategy for the NSTX poloidal velocity measurement. The chosen viewing geometry exploits plasma symmetry to directly measure line-integrated poloidal flow, avoiding complex atomic physics corrections. High throughput optics and high quantum efficiency detectors are used to improve the accuracy of the velocity measurement. An inversion procedure is used to obtain the local poloidal velocity profiles. The high radial resolution available with the pre-existing toroidal viewing system was preserved with the poloidal viewing system. The NSTX design is similar in many respects with the TFTR poloidal velocity diagnostic,[2] both providing symmetric views from above and below the midplane.

II. VIEWING GEOMETRY

NSTX is a spherical torus with a major radius of 0.85 m and a minor radius of about 0.6 m, magnetic fields of 0.3–0.55 T, and plasma currents of up to 1.8 MA, with plasma discharges of up to 1.8 s. The neutral beams provide up to 6 MW of auxiliary heating. The three horizontally directed neutral beam sources are located at one tangential port on NSTX. Each source is nominally 12 cm wide and 42 cm tall. The beam source trajectories intersect near the plasma edge and have an angular separation of about 4° (see Fig. 1). The interior walls of NSTX are largely covered with carbon tiles, making carbon the dominant impurity. The charge exchange recombination spectroscopy (CHERS) system on NSTX uses the n=8–7 transition of the C^{5+} ion at 529.1 nm to infer the temperature, density, and velocity of the parent ion C^{6+}. Along with the charge exchange emission, intrinsic background emission from C^{5+} ions is also present. Dedicated views that do not intersect the beam are used to measure this background emission. The technique of modulating the neutral beam to subtract the background emission is not practical for most experiments on NSTX since it would require modulating 100% of the beam power. Both poloidal and toroidal viewing CHERS systems are used on NSTX. The poloidal viewing system is sufficient to measure line-integrated velocity. To obtain local measurements, an inversion is performed, which requires information from the toroidal viewing system. Collection optics mounted on NSTX couple light into sets of optical fibers approximately 35 m long, which connect to spectrometers located in a remote diagnostic room.

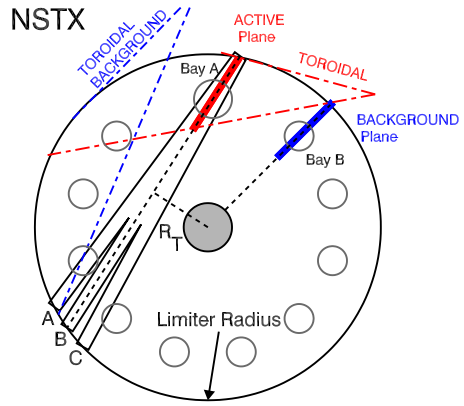

FIG. 1. (Color online) Plan view of NSTX midplane showing the locations of the active and background detection planes for the poloidal views. The active plane shares the same tangency radius (RT) as the central beam. Also shown are the range of the toroidal views and the corresponding background views.

A. Midplane toroidal views

The toroidal viewing system is situated at the plasma midplane. Two sets of sightlines view across the neutral beams and parallel to the neutral beams to provide active measurements and simultaneous independent background measurements (see Fig. 1). The active view has 102 fibers, each 210 μm in diameter, which are paired to provide 51 spatial channels across the midplane. The radial resolution is variable, about $\Delta r=0.6$ cm near the edge and increasing to about $\Delta r=3.0$ cm in the core. With the low magnetic field typical of the spherical torus, the edge resolution is comparable to the ion gyroradius. The toroidal viewing optics is shared with the motional Stark effect (MSE) diagnostic.[3] A 3 cm aperture is mounted on the shared 25 cm diameter $f/1.2$ lens to restrict the Doppler widths observed by the MSE diagnostic, which also reduces the throughput available for the CHERS system. Intrinsic background emission is imaged by an 85 mm $f/1.8$ Nikon lens onto 39 fibers 600 μm in diameter. This viewing lens is shared by the toroidal views of the edge Doppler spectrometer,[4] which measures emission from C^{2+}, He^{+}, Li, and Li^{+}, and another visible spectrometer.

B. Up/down symmetric poloidal views

The poloidal viewing CHERS system was designed to have matched symmetric views from above and below the plasma. The upper and lower sightlines are precisely aligned where they intersect at the midplane (see Fig. 2). The active plane of measurement is aligned with the central neutral beam trajectory. The horizontal distance along this detection plane, $X=(R^2-R_T^2)^{1/2}$, can be defined in terms of the major radius R and the tangency radius of the plane R_T. Nonvertical sightlines in this plane will have a slight toroidal component contributing to the apparent velocity. The background emission is measured in a radial plane at a toroidal location about 30° from the neutral beams (see Fig. 1). Higher resolution is

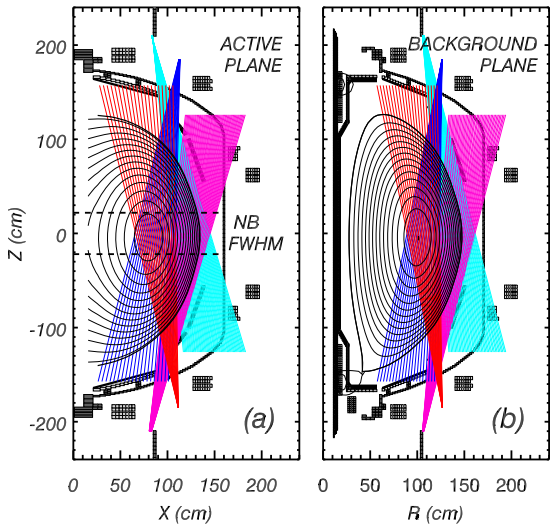

FIG. 2. (Color online) Cross sections of NSTX showing poloidal viewing sightlines in (a) active plane and (b) background plane. Each of the 138 pairs of upward and downward viewing sightlines is precisely aligned at the midplane.

provided in the outer portion of the plasma ($R \geq 120$ cm) with twice as many sightlines. The radial resolution after inversion is $\Delta r = 0.6$ cm in the outer range and $\Delta r \leq 1.8$ cm near the plasma center, comparable to the toroidal viewing system.

The sequential layout of the top and bottom ports was altered, at time of the vacuum vessel design, to accommodate a vertical view of the neutral beams for a poloidal velocity measurement. The typical vertical port uses a 13.25 in. flange aligned with the gaps between passive plates. Larger ports (16.5 in flanges) were positioned above and below the neutral beam location to provide symmetric views along the neutral beam trajectory that intersect the midplane from inside the magnetic axis outward beyond the plasma edge. The detection plane for the active charge exchange emission is tangential and centered on the neutral beam trajectory. For the background emission, a standard port is used along a radial plane located away from the neutral beam. Two viewports with 5.25 and 4 in. windows were used on the large flange viewing the beam (see Fig. 3). A custom oval window was designed for the smaller flange to accommodate the collection optics.

Custom designed shutters mounted on the flanges protect the viewing windows. A pair of rotary pneumatic actuators is mounted on each of the larger flanges to control the horizontal rotation of shutters in front of the window. A linear pneumatic actuator on the smaller flange couples to a shutter plate that rotates to a position perpendicular to the flange when the shutter is open and parallel to the flange when the window is covered. These shutters are part of a much larger system of diagnostic shutters on NSTX that are interlocked to the plasma operation sequence.

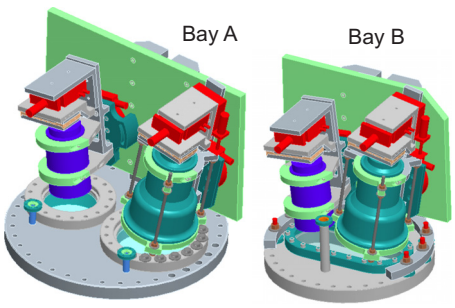

FIG. 3. (Color online) Computer-aided design rendering of the port flanges and the lens mounting hardware.

Gaps in the passive plates are aligned with the standard port locations for vertical views of the plasma. The ports above and below the neutral beam were blocked by the initial passive plate installation. A redesign of the plates was necessary to accommodate unobstructed vertical views for the poloidal velocity measurement. Electrical continuity of the passive plates was retained with a curved plate replacing the portion of the passive in the viewing path, and flux loops were rerouted out of the path of the view.

III. COLLECTION OPTICS AND FIBERS

The design of the poloidal viewing system attempts to preserve the high radial resolution already available with the toroidal viewing system. The number of sightlines required more than doubles since atomics physics considerations required views of the neutral beam from both top and bottom. Optically fast lenses are also required to match the spectrometer. Two commercial lenses are positioned on each flange to image the plasma onto fiber optics. A Canon 200 mm $f/1.8$ lens is used to view the outer radii. A Nikon 135 mm $f/2.0$ lens is used for the core views. The upper and lower flanges are located about 1.8 m from the midplane. The magnification of the fibers at the midplane is about 8.7 for the 200 mm lens and about 13.3 for the 135 mm lens. Optical fibers with a 400 μm core diameter are used in the active viewing plane with the 200 mm lens. For the background sightlines and the active sightlines in the core, 600 μm diameter fibers are used. With the 200 mm lens, the image sizes of the fibers at the midplane are 3.5 and 5.2 mm for the 400 and 600 μm fibers, respectively. With the 135 mm Nikon lens, the image of the 600 μm fibers is about 8 mm at the midplane. The fibers are mounted in custom holders behind the lens. Due to space limitations at the installation location, a mirror is mounted behind the lens so that the fibers can be mounted perpendicular to the optical axis of the lens. The lens mounts are designed to allow the direction of the lenses and the position and orientation of the fibers to be adjusted for alignment (see Fig. 3). The 135 mm lens has a manual adjustment. Adjusting the position of the fibers with a translation stage focuses the 200 mm lens. The collection optics for the poloidal CHERS system are shared with a fast ion D-alpha diagnostic[5] and the poloidal views of an edge Doppler instrument.[4]

A total of 276 optical fibers is used with the eight lenses. 75 pairs of fibers are viewed in the active plane (54 at 400 μm and 21 at 600 μm) and 63 pairs of fibers are viewed in the background plane. The 35 m long optical fibers are sleeved in a nylon mesh and bundled in protective corrugated tubing. The fibers conduct light from the collection optics outside the experimental test cell to a diagnostic area. The input ends of the fibers are bare and mounted on the

fiber holders and the output ends of the fibers are terminated with SMA connectors and attached to a patch panel. The fiber transmission for a 35 m length of fiber at 530 nm was 75%, measured at a numerical aperture of 0.3.

IV. SPECTROMETERS AND DETECTORS

The spectrometers for both toroidal and poloidal CHERS systems are Holospec™ $f/1.8$ spectrometers, manufactured by Kaiser Optical Systems, Inc., along with their high dispersion grating (HDG). A number of enhancements to the commercial instrument have been made to improve the performance of these spectrometers.[6] The output lens was modified to a 58 mm $f/1.2$ Nikon lens, which, along with the standard 85 mm input lens, demagnifies the image of the input fibers on the detector while preserving étendue. This allows more input fibers to be placed vertically at the entrance slit. Instead of a single entrance slit, three horizontally displaced slits are used, tripling the number of input fibers. These slits are curved to produce straight images at the detector. A narrow bandpass filter is mounted onto the input lens to prevent overlap of the adjacent spectra. The bare ends of short (4 m) fibers with SMA termination are potted into a custom slit plate and polished by the fiber manufacturer, Fiberguide Industries. The SMA connector attaches to the patch panel mentioned above. Laser cut slits are mounted on a plate. The fiber plate and the slit plate are stacked onto a standard kinematic slit mount for the Holospec instrument. The number of spectra in a spectrometer depends on the fiber size, 54 spectra for 400 μm fibers and 42 spectra for 600 μm fibers. Six spectrometers can accommodate all 276 optical fibers of the poloidal viewing CHERS.

Fiber placement on the detector is flexible since a patch panel system is used. To facilitate good differential velocity measurements, the corresponding fibers from upper and lower views are placed symmetrically about the center of each slit. In this way, half of the fibers in a spectrometer are from upward viewing sightlines and half are from a downward viewing sightline. This results in identical dispersion for matching sightlines and provides the most stable relative measurement of wavelength shift.

The detector used is a PhotonMax frame transfer CCD camera, manufactured by Roper Scientific, Inc., which has a 512×512 array of 16 μm pixels. The thinned backilluminated charge-coupled device (CCD) provides 95% quantum efficiency at 529.1 nm. The camera digitizes to 16 bits at 5 or 10 MHz. Vertical binning is performed on the chip to decrease readout time. For the CHERS diagnostics, the cameras are operated at 100 Hz frame rate. A dedicated computer controls each camera. A chopper with two tabs spinning at 50 Hz is synchronized with the camera readout to mask the CCD during the frame transfer to prevent smearing of the image. The tab width on the custom chopper blade is sized to include the time for the frame transfer, transit time across the CCD face, and uncertainty in the chopper phase. For the poloidal CHERS, the net exposure time is 7.4 ms out of a 10 ms frame time. The chopper is operated with a SciTec Instruments chopper controller and synchronizer. A 100 Hz signal pulse, which is synchronized to the NSTX master clock, is provided for chopper timing. A Computer Automated Measurement and Control (CAMAC) controlled module determines the timing window for a corresponding train of clocking signals to the CCD camera external sync input.

V. ALIGNMENT AND CALIBRATION

For the narrowest instrumental width, the CCD detector should be centered on and normal to the optical axis of the spectrometer. The alignment of the CCD detector to the spectrometer is accomplished with a six-axis adjustment. The CCD camera is not directly connected to the spectrometer. The spectrometer is mounted on an X-Y translation stage, which serves to align the spectra with the CCD and to focus the image. The detector is mounted on a three-axis rotation stage atop a vertical translation stage. After an initial optical alignment, fitted linewidths from a calibration spectrum are monitored as the instrumental width is optimized across the detector.

The careful alignment of fibers for the poloidal view is critical for the poloidal sightlines since the symmetry is needed to cancel the atomic physics contributions to the measurement. A reference line on the midplane that extends along the path of the central neutral beam source is located. A steel rule is placed on this line, indicating the position along the beam path. With backilluminated fibers, one lens of an up/down pair is adjusted so that the images of the fibers fall on the desired positions along the reference line. Next, the matching lens is adjusted so the fiber images coincide with those of the first lens. This process is repeated for each of the four pairs of lenses. The lens mount (see Fig. 3) allows a rotation of the lens along the detection plane. The fiber holder can be rotated about the viewing axis and translated laterally. Together, these adjustments allow precise control of the sightline direction. After alignment, the adjustments are locked down.

An articulated measuring arm manufactured by Faro Technologies is used for precise measurements inside the vacuum vessel. The position of a pointer can be determined in three dimensions with submillimeter accuracy. Monuments (steel balls) fastened to the inside of the vessel serve as reference points to establish the coordinate system for a measurement. This tool is used to establish the position of the neutral beam trajectory mentioned above and to measure the location of the backilluminated fiber images once the alignment is complete.

After alignment, a spatial calibration is performed. The image of a fiber intersecting a plane is an ellipse. Points around the ellipse are measured and those points are fit regressively using software of the measuring arm to produce a central location with an accuracy better than the individual measurements. The position of the fiber images is measured on a set of planes along their paths. The path of each sightline is then fit in three dimensions. A regression is then performed on all of the fitted lines to determine the best fit for a single virtual point (see Fig. 2) from which all the sightlines from a particular lens emanate. This virtual point is then used to refit the lines of each sightline with an accuracy better than the individual line fits. The path of the sightlines is thus

determined to better than 0.01°. Once aligned, the fiber alignment seems to be quite stable. Calibrations before and after an operational period show the deviation in the measured positions where the sightlines intersect the midplane deviated less than a millimeter. A 1 mm displacement in the toroidal direction would correspond to less than a 0.2 km/s contribution from a toroidal velocity of 350 km/s, which is the maximum velocity measured on NSTX.

A photometric calibration is also done inside the vacuum vessel. A curved white plate with a Lambertian reflecting surface is illuminated by a pair of quartz lamps positioned at the center of curvature of the plate. The lamps are illuminated using a regulated dc source. The white plate is positioned in front of each set of sightlines and illuminated while a set of data is recorded, which gives a relative photometric calibration for all fibers. A subset of fibers is then exposed to an absolutely calibrated integrating sphere. The comparison of signals between the white plate and the calibrated integrating sphere cross calibrates the white plate at the wavelength of the spectrometer, giving an absolute calibration to all fibers previously calibrated with the white plate.

The last calibration is performed after the initial plasma operation. A glow discharge is established using neon gas in the vacuum vessel. The diffuse glow illuminates the collection optics and fibers as the plasma would, including any vignetting due to the viewing geometry. Two neon lines at 529.82 and 530.48 nm are used for wavelength and instrumental function calibrations for the CHERS spectrometers. The pair of lines is fit with single, double, and triple Gaussians. The best of these fits in each case is used for the instrumental function for that channel. A linear wavelength calibration is determined from the best fit of neon line pair.

VI. DATA ACQUISTION AND ANALYSIS

The six local computers for the poloidal CHERS system and the two local computers for the toroidal CHERS system run the same VISUAL BASIC routine. They are coordinated through a central Interactive Data Language (IDL) program on another computer running under a different operating system. The data management system used on NSTX is MDSPLUS,[7] which has an event feature convenient for communicating across disperse computer platforms. The graphical user interface (GUI) running an IDL program monitors machine event cycles and transmits a unique MDS event for each PC running a CHERS camera a minute before the discharge start. The individual computers then ready the camera for acquisition a few seconds before the discharge. The trigger timing for the cameras is set with the CAMAC hardware, which is also initialized by the MDSPLUS system at the start of the shot cycle. All the CHERS cameras are triggered simultaneously by external triggers. After the discharge, the local computers write the data to the MDSPLUS tree, usually within 6 s of the discharge. Each local computer then sends another MDS event, which is monitored by the GUI, signaling the status of the acquisition and data storage. Timing information for the camera triggers and the chopper phase are recorded in CAMAC and stored on the MDSPLUS tree within 30 s of the discharge.

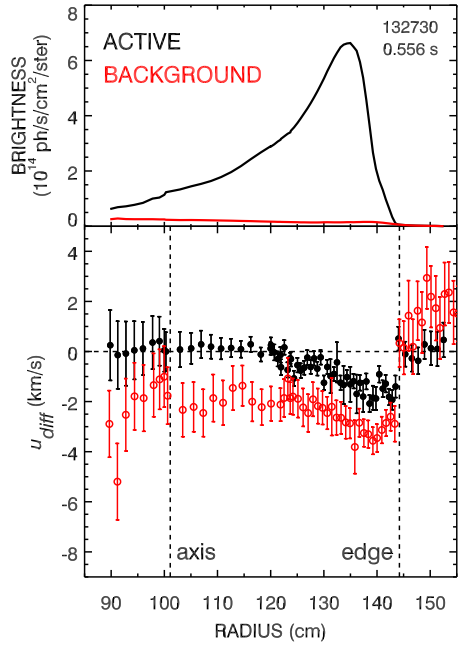

FIG. 4. (Color online) In the upper panel are examples of the brightness profiles of the active (black) and passive (red) views. In the lower panel are the line-integrated differential velocity profiles of the active (solid) and passive (hollow) views. The vertical dashed lines indicate the magnetic axis and the plasma edge.

After the discharge, when the CHERS and neutral beam timing are available, the GUI automatically starts a batch job to fit the toroidal CHERS data. When data from Thomson scattering and neutral beam power and voltage are available, the fitted toroidal CHERS data are analyzed. This includes a beam attenuation calculation, correction for the energy-dependent charge exchange cross section, and a Zeeman correction. The fully analyzed data (ion temperature, carbon density, toroidal velocity, etc.) are then written to the MDSPLUS tree, usually within 4.5 min of the discharge end.

The analysis of the poloidal CHERS data is not yet automated.[8] It is computationally more intensive and will require analysis on multiple processors to be available between shot cycles. The increased computation time is related to the number of spectra, the required two-dimensional beam attenuation correction, and the two-dimensional computation of effective charge exchange emissivity.

VII. RESULTS

Differential velocity measurement using matched pairs of upward and downward viewing sightlines are used to remove the unwanted horizontal velocity components. These include components of the toroidal velocity for nonvertical sightlines and the net flow toward the neutral beam due to the energy-dependent charge exchange cross section. Since the gyro orbit finite lifetime effects are small, this gives the line-integrated poloidal velocity. The view through the active plane of measurement yields a composite of the charge exchange (CX) emission and background emission. The background emission alone is measured in the other detection plane. Figure 4 shows an example of the line-integrated velocity profiles in the active and background planes along with the associated brightness profiles. This particular dis-

charge employs three neutral beams so the signal to background is large. The $f/1.8$ spectrometers are typically operated at $f/2.8$ or $f/4$ for the active viewing system to avoid saturation.

A matrix inversion technique[8,9] is applied to obtain the line-integrated CX emission and the local poloidal velocity measurement. An equilibrium reconstruction is used with the assumption that the emissivity of the background emission is constant on a flux surface. A matrix to obtain line-integrated brightness from local emissivity can be inverted to obtain emissivity from brightness measurements. By adding directional information to the line matrix, a similar inversion can obtain emissivity weighted local velocity from brightness weighted line-integrated velocity. The method is briefly described below (see Refs. 8 and 9 for details).

To compute the contribution from the CX emission alone, the following relationship is used to compute the brightness weighted velocity for the charge exchange emission:

$$B^{\mathrm{CX}}u^{\mathrm{CX}} = B^{\mathrm{tot}}u^{\mathrm{tot}} - B^{\mathrm{BKG}}u^{\mathrm{BKG}}, \quad (1)$$

where B^{tot} and u^{tot} are the brightness and line-integrated velocity for the active view, and B^{BKG} and u^{BKG} are the corresponding values for the background. These background values are determined by applying a matrix inversion on the background measurements to obtain local background measurements, interpolating to the active measurement locations (see X versus R in Fig. 2), and then recomputing the line-integrated background measurements for the active plane view.

The quantity $B^{\mathrm{CX}}u^{\mathrm{CX}}$ is then used to obtain local values of poloidal velocity. To invert these data, knowledge of the emission along the sightlines is required. This is supplied by the local toroidal CHERS measurements and local Thomson scattering measurements.[10] Midplane measurements are mapped into two dimensions in the active detection plane using the flux surfaces from the equilibrium construction. The mapped quantities are used in a two-dimensional beam attenuation calculation, which gives the local beam neutral density. A local charge exchange cross section is also computed. A weighted emissivity in two dimensions is then computed from the product of the beam neutral density, the carbon density, and the effective charge exchange cross section. This information is put into matrix form in a manner similar to the background inversion, one matrix relates line-integrated brightness to the local computed CX emissivity and another contains the angular information of the components of velocity along the sightline. The ratio of these inverted matrices gives the local poloidal velocity. Measurement errors are propagated through the calculation. An example of an inverted poloidal velocity profile is shown in Fig. 5. The inverted profile remains quite similar to the active view line-integrated velocity because there is little or no central rotation and no sharp gradients.

The ability to measure the poloidal velocity profile now completes the previously available toroidal CX measurements of C^{6+} needed to determine the radial electric field using the force balance equation. The measurement approach taken here relies on carefully aligned symmetric views to extract a line-integrated poloidal velocity without invoking complex atomic physics corrections. In order to obtain local measurements, atomic physics data were used on the toroidal measurements to correct principally for the toroidal velocity, which is relatively large (200 km/s for the example shown in Figs. 4 and 5). The computed charge exchange emissivity was used in a relative sense to extract the local values. Details of the energy-dependent charge exchange cross section, particularly at low collision energies, may carry uncertainties that could adversely affect the much smaller inferred poloidal velocity. (In the example shown, the poloidal velocity is more than two orders of magnitude smaller than the toroidal velocity.) On NSTX, the magnitude of the gyro orbit finite lifetime effects can be neglected, but on higher temperature plasmas with higher magnetic fields, it can dominate the poloidal velocity. With symmetric views, the vertical and horizontal components of velocity could be distinguished. Knowing the net CX flow toward the beam, the local magnetic field, and the lifetime of the excited state would allow the extraction of poloidal flow without atomic physics corrections in the conditions where the gyro orbit effects cannot be ignored.[1]

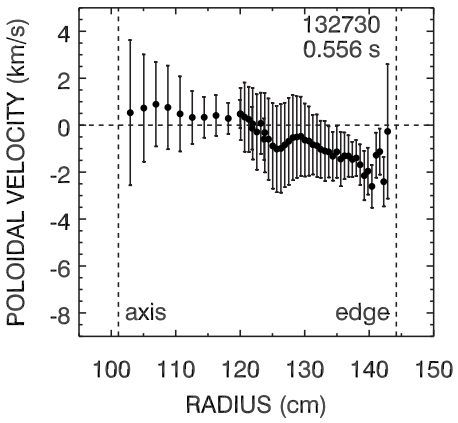

FIG. 5. Local poloidal velocity profile after inversion.

ACKNOWLEDGMENTS

The authors would like to acknowledge the assistance of J. Carson in preparing the fiber optics. The support of D. W. Johnson and B. C. Stratton is appreciated. This work was supported by the U. S. Department of Energy under Contract No. DE-AC02-09CH11466.

[1] R. E. Bell and E. J. Synakowski, AIP Conf. Proc. **547**, 39 (2000).
[2] R. E. Bell, L. E. Dudek, B. Grek, D. W. Johnson, and R. W. Palladino, Rev. Sci. Instrum. **70**, 821 (1999).
[3] F. M. Levinton and H. Yuh, Rev. Sci. Instrum. **79**, 10F522 (2008).
[4] T. M. Biewer, R. E. Bell, R. Feder, D. W. Johnson, and R. W. Palladino, Rev. Sci. Instrum. **75**, 650 (2004).
[5] M. Podestà, W. W. Heidbrink, R. E. Bell, and R. Feder, Rev. Sci. Instrum. **79**, 10E521 (2008).
[6] R. E. Bell, Rev. Sci. Instrum. **75**, 4158 (2004).
[7] J. A. Stillerman, T. W. Fredian, K. A. Klare, and G. Manduchi, Rev. Sci. Instrum. **68**, 939 (1997).
[8] R. E. Bell, R. Andre, S. M. Kaye, R. A. Kolesnikov, B. P. LeBlanc, G. Rewoldt, W. X. Wang, and S. A. Sabbagh, Phys. Plasmas **17**, 082507 (2010).
[9] R. E. Bell, Rev. Sci. Instrum. **68**, 1273 (1997).
[10] B. P. LeBlanc, R. E. Bell, D. W. Johnson, D. E. Hoffman, D. C. Long, and R. W. Palladino, Rev. Sci. Instrum. **74**, 1659 (2003).